# Response of Earth's neutral sheet to reversals in the IMF $B_y$ component

**N. A. Case[1], A. Grocott[1], S. Haaland[2,3], C. J. Martin[1], T. Nagai[4]**

[1]Department of Physics, Lancaster University, Lancaster, UK.
[2]Max Planck Institute for Solar System Research, Göttingen, Germany.
[3]Department of Physics and Technology, University of Bergen, Norway.
[4]Institute of Space and Astronautical Science, Sagamihara, Japan.

**Key Points:**

- The statistical response of the neutral sheet to reversals in the IMF $B_y$ component is demonstrated
- Individual responses of the neutral sheet to IMF $B_y$ reversals are investigated
- The inner magnetosphere neutral sheet responds rapidly to IMF $B_y$ reversals

Corresponding author: N. A. Case, n.case@lancaster.ac.uk

## Abstract

The $B_y$ component of the interplanetary magnetic field (IMF) plays an integral part in the coupling of the solar wind-magnetosphere-ionosphere system. In this study, we use a suite of magnetospheric spacecraft, with data spanning nearly 25 years, to statistically investigate the control of the IMF $B_y$ component on the neutral sheet. Past studies have identified that this thin layer of the magnetotail, which separates the oppositely directed magnetotail lobes, responds to reversals in the IMF $B_y$ component. The proposed method for driving this response is through unequal flux loading in the magnetotail lobes and we present lobe flow data from the Cluster mission which suggests that this is indeed the case. We find that the neutral sheet responds in a statistical fashion, with a clear twist or rotation whose orientation depends upon the polarity of the IMF $B_y$ component. Additionally, under individual analyses, we find the response time of the neutral sheet to IMF $B_y$ reversals is much shorter than possible through the classical dayside reconnection driven picture. We find an average response time of between 10-20 min with little to no dependence on distance down tail. These results suggest that the neutral sheet responds to the IMF $B_y$ component on multiple timescales.


## 1 Introduction

First detected by *Ness* [1965], using measurements from the IMP 1 satellite, Earth's neutral sheet separates the tailward directed magnetic field in the southern hemisphere from the earthward field in the northern hemisphere. This relatively thin region of space, located within the plasma sheet, is characterized by a strong cross tail current, a minimum in the total magnetic field intensity, and a reversal in the local $B_x$ magnetic field component [*Speiser and Ness*, 1967].

The average location and shape of the neutral sheet has been studied extensively in the past [e.g. *Fairfield*, 1980; *Hammond et al.*, 1994; *Tsyganenko and Fairfield*, 2004; *Xiao et al.*, 2016] and these studies have demonstrated that the neutral sheet is not static. Its position and configuration vary with local factors, such as the dipole tilt angle, and with the external driving of the solar wind and the embedded interplanetary magnetic field (IMF). Such factors introduce a warping, bending, and twisting of the neutral sheet [*Zhang et al.*, 2002]. In this study, we focus particularly on the effect of the IMF $B_y$ component on the neutral sheet.

It is well known that the IMF $B_y$ component induces a $B_y$ component into the magnetosphere [e.g. *Cowley and Hughes*, 1983; *Kitaev*, 1993; *Wing et al.*, 1995; *Tenfjord et al.*, 2015] and, as such, is the source of several asymmetries throughout the magnetospheric and ionospheric systems [e.g. *Grocott et al.*, 2007]. A non-zero IMF $B_y$ component results in the site of dayside reconnection moving from the subsolar point toward the high-latitude flanks [*Park et al.*, 2006]. This, in turn, results in asymmetric flux loading of the lobes [*Cowley*, 1981]. As described in *Tenfjord et al.* [2016], there are then two methods by which a $B_y$ component is induced into the closed magnetosphere.

Firstly, the asymmetric flux loading results in magnetic pressure building up in the lobes. As first suggested by *Khurana et al.* [1996], this generates shear flows in the magnetosphere which are oppositely directed in the two hemispheres. These shear flows result in the rapid induction of a $B_y$ component on the already present closed field lines in the magnetosphere [*Tenfjord et al.*, 2015]. Secondly, as first proposed by *Russell* [1972] and *Cowley* [1981], the asymmetric flux results in asymmetric nightside reconnection of open field lines which exerts a torque in the magnetotail. This torque produces a twist which, in turn, results in the induction of a $B_y$ component in the closed magnetotail field lines. Specifically, intervals of $B_y > 0$ driving should induce an anti-clockwise twist (when visualized looking downtail from Earth). Later studies, e.g. *Sibeck et al.* [1985]; *Nagai* [1987]; *Owen et al.* [1995]; *Nishida et al.* [1998], found that this was indeed the case.

Numerous studies have looked into the timing of the induced $B_y$, using ionospheric responses, shear flows, tail twisting, and cross correlation studies [e.g. *Tenfjord et al.*, 2016; *Rong et al.*, 2015; *Browett et al.*, 2016]. However, previously, only case-studies into the response time of the neutral sheet to changes in the IMF have been undertaken [e.g. *McComas et al.*, 1986; *Motoba et al.*, 2011; *Rong et al.*, 2015; *Pitkänen et al.*, 2016]. We note that previous studies, e.g. *Nagai* [1987] and *Tenfjord et al.* [2016], have performed statistical analyses of the induced $B_y$ component but these studies were restricted to the inner magnetosphere.

In this study, using nearly 25 years worth of magnetospheric magnetic field data, we undertake a statistical analysis of the response of the neutral sheet to changes in the IMF $B_y$ component orientation. Additionally, through individual event analyses, we find the response time of the neutral sheet to reversals in the IMF $B_y$ component.

## 2 Data Selection

At its simplest, the magnetotail neutral sheet is what separates the tailward orientated magnetic field, i.e. negative $B_x$ (in a geocentric-solar coordinate system), from the earthward directed field, i.e. positive $B_x$. Therefore, to determine its position statistically, one need only find where the direction of the x-component of the magnetic field reverses [*Tsyganenko et al.*, 1998]. To do this simply requires in situ magnetic field measurements from the region of interest.

In this study, we utilize magnetic field data from a suite of spacecraft missions: Geotail (1992-2016) [*Kokubun et al.*, 1994], Cluster (2001-2015) [*Balogh et al.*, 1997], THEMIS (2007-2016) [*Auster et al.*, 2009], and Double Star (2004-2007) [*Carr et al.*, 2005]. Additionally, we use Cluster's electron drift instrument (EDI) [*Paschmann et al.*, 1997] to determine plasma convection in the magnetotail lobes.

All data are re-sampled to one minute cadence and are converted into the geocentric solar wind (GSW) coordinate system [*Hones et al.*, 1986] to account for the solar wind aberration effect on the magnetotail. The GSW coordinate system is similar to the aberrated geocentric solar-magnetospheric (AGSM) system but differs from it by using the solar wind velocity to determine the actual aberration angle - rather than assuming a constant aberration angle of 4°.

Furthermore, the location data of the spacecraft are normalized by solar wind dynamic pressure. Using the technique of *Hammond et al.* [1994], we attempt to account for the effect of the solar wind dynamic pressure on the size of the earth's magnetotail and normalize the location of the spacecraft within it. As shown in equation 1, the normalization factor ($\eta$) takes the form of a simple one sixth power scaling with respect to a "reference" dynamic pressure ($p_r$):

$$\eta = (p_m/p_r)^{\frac{1}{6}} \tag{1}$$

where $p_m$ is the measured dynamic pressure (which we compute as the average value over the previous hour). We choose the reference pressure to be the mean dynamic pressure for all solar wind data within the time period of this study, i.e. 1992-2016, and we find this to be 2.10 nPa.

If the impinging dynamic pressure is stronger than the reference pressure (i.e. $p_m > p_r$) the location of the spacecraft is scaled closer to the Earth to account for the dynamic pressure compressing the magnetosphere. Conversely, if $p_m < p_r$ the spacecraft location is scaled further away from the Earth to account for an expanded magnetosphere.

Solar wind and IMF data are collated from NASA's high-resolution (1 min) OMNIweb database [*King and Papitashvili*, 2005]. The OMNIweb database provides a convenient

source of solar wind and IMF data that has been propagated to the Earth's bowshock with a good degree of accuracy [*Case and Wild*, 2012]. The database is an amalgamation of data from various upstream satellite missions, including WIND, ACE and DSCOVR.

Magnetic field data collected near the neutral sheet (i.e. bounded by the region $-50 \leq X_{GSW} < 0\,R_E$, $|Y_{GSW}| \leq 30\,R_E$, and $|Z_{GSW}| \leq 3\,R_E$) are selected from each of the spacecraft and combined into one large dataset. Beyond $50R_E$ downtail data coverage is too poor for statistical analysis with this dataset. The spatial coverage of the combined magnetic field data is shown in Figure 1. The amount of data in each bin is presented in days (where one day equates to 1,440 data points at one minute resolution). The particularly high density region ($5 < r < 15\,R_E$) is the result of the elliptical orbits of the four Cluster spacecraft.

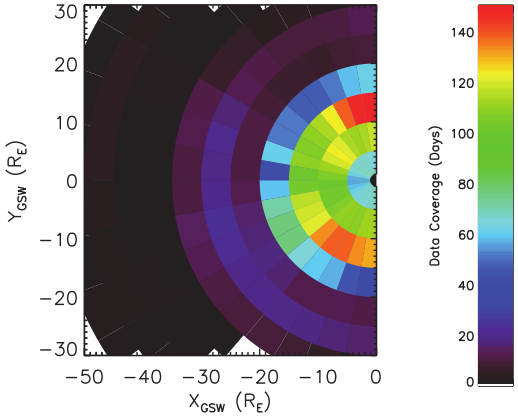


**Figure 1.** The number of combined data in each spatial bin, converted from one minute resolution counts into "days", is shown. The higher density coverage in the inner magnetotail is due to the elliptical orbital configuration of the four Cluster satellites.

We note that the data are fairly evenly distributed above and below the neutral sheet, with 51.0% of the data being recorded between $0 < Z_{GSW} < 3R_E$ and thus 49.0% between $-3 < Z_{GSW} \leq 0R_E$. There is, however, some X dependence to this distribution, with more data located in $Z_{GSW} < 0$ the further downtail it was recorded ($\sim 60\%$ at $-40R_E$).

## 3 Results and analyses

In the following section, we investigate both the effect of the average IMF $B_y$ orientation on large-scale morphology of the neutral sheet, as well as the response time of the neutral sheet to reversals in the IMF $B_y$ orientation.

### 3.1 Average morphologies

For each magnetospheric magnetic field data point located within the region of interest, the modal IMF clock angle ($\theta$) orientation for the preceding 60 min is determined. We chose a value of 60 min as this order of response time is sufficient for a large-scale response of the tail to take place [e.g. *Browett et al.*, 2016] and produce the *Cowley* [1981] twist.

The modal values are then grouped into the following 45°-wide classifications, centered on the cardinal and intercardinal directions: north ($\theta \geq 337.5°$ and $\theta < 22.5°$), north-east ($67.5° > \theta \geq 22.5°$), east ($112.5° > \theta \geq 67.5°$), south-east ($157.5° > \theta \geq 112.5°$), south ($202.5° > \theta \geq 157.5°$), south-west ($247.5° > \theta \geq 202.5°$), west ($292.5° > \theta \geq 247.5°$), and north-west ($377.5° > \theta \geq 292.5°$). So that we only include intervals where the clock angle is

stable, data intervals with less than 60% agreement between individual clock angles and the modal classification are discarded.

In Figures 2 and 3, the magnetotail magnetic field data are grouped by their corresponding IMF clock angle orientation. For each orientation the associated magnetic field data are binned into 5 $R_E$ by 10° bins. The median value of the local magnetic field component in each bin determines the bin's color with the same color scale being used across all panels. Shown in Figure 2 is the local $B_x$ component and in Figure 3 is the local $B_y$ component.

Since the region of interest spans only $\pm 3\,\mathrm{R_E}$ in the $\mathrm{Z_{GSW}}$ direction, we are in effect looking at the slice of space containing the neutral sheet. Assuming that the neutral sheet is indeed located on the equatorial plane, the median $B_x$ value should equate to zero. That is, there should be an equal amount of tailward field (negative $B_x$) and earthward field (positive $B_x$). Any deviation from this equality demonstrates non-uniformity and, if this deviation is a systematic change from positive to negative azimuthally across the tail, it is indicative of a twisting or rotation of the neutral sheet. We note that small, short-lived, disturbances to the neutral sheet (e.g. warping and bending) will average out over such a large data set.

Figure 2 demonstrates that there is a statistical preference for positive $B_x$ in the post-midnight sector, and negative $B_x$ in the pre-midnight sector, under eastward IMF ($B_y > 0, |B_y| > |B_z|$) conditions. This trend is reversed under westward IMF ($B_y < 0, |B_y| > |B_z|$) conditions. This is consistent with the idea of a neutral sheet twist. Figure 3 clearly demonstrates that the local $B_y$ orientation does indeed match that of the IMF $B_y$ component.

To test the suggestion that this preference relates to the unequal loading of IMF in the lobes [e.g. *Haaland et al.*, 2008], we also plot the plasma convection in the lobes for eastward and westward IMF in Figure 4. The convection data, provided by the Cluster EDI instruments, are binned using the same criteria as for the magnetic field data in Figure 2. We first discard any flow velocities of $>100\,\mathrm{kms^{-1}}$ as these are determined to be anomalous [*Haaland et al.*, 2008]. We then compute the mean $V_x$ and $V_y$ components of the convection velocity for each bin, and use them to determine the magnitude and direction of $V_{xy}$, where $V_{xy} = \sqrt{{V_x}^2 + {V_y}^2}$. The length of the arrow in each bin of Figure 4 represents the magnitude of $V_{xy}$ and the color represents the number of data points in that bin.

Figure 4 clearly demonstrates that, in the Northern Hemisphere lobes, eastward IMF ($B_y > 0$) drives duskward flows and westward IMF ($B_y < 0$) drives dawnward flows. The directions are reversed in the Southern Hemisphere. As described in detail in *Haaland et al.* [2008], this is consistent with asymmetric flux loading from the dayside. For example, under $B_y > 0$ conditions in the Northern Hemisphere, recently opened field lines convect dawnwards under the effect of the tension force (the so-called Svalgaard-Mansurov effect, as summarised in *Wilcox* [1972]) and are thus deposited preferably in the dawn side of the lobe. This subsequently excites duskward flow within the lobe as the asymmetric pressure distribution is equalised between the dawn and dusk lobes (see Figure 6 in *Haaland et al.* [2008]).

We note that there is a significant difference in the quantity of Cluster EDI data collected between the Northern and Southern hemispheric lobes. This bias is simply due to the orbital configuration of the Cluster satellites preferentially sampling the Southern Hemisphere lobe over the Northern Hemisphere lobe. No such bias exists in Figure 2 since we sample the neutral sheet region, rather than the lobes.

To explore these relationships further, and determine the statistical response time of the neutral sheet to changes in the IMF $B_y$ component, we analyse the local $B_x$ data in the neutral sheet region under intervals of IMF $B_y$ reversal.

### 3.2 IMF $B_y$ reversals

To determine the response time of the neutral sheet to reversals in the IMF $B_y$ component, we first determine when the orientation of the IMF $B_y$ component reverses. To do this, we employ a method similar to *Tenfjord et al.* [2016]. For each IMF data point, we compute a 20 min and a 60 min average, both forward and backward in time. A reversal from positive to negative $B_y$ is said to have occurred if both the 20 min and 60 min backward averages are $> 2$ nT and both the forward averages are $< -2$ nT (and vice versa for negative to positive). We compute the two differing length averages to ensure a stable pre- and post-transition period (60 min average) with a prompt transition (20 min average).

These reversal criteria were applied to the OMNI data set for years 1992 - 2016 and resulted in the identification of 6,825 IMF $B_y$ reversals. We then selected only those with coincident magnetotail magnetic field data, leaving 2,794 reversals. Of these, 1,377 (49.3%) were positive to negative and 1,417 (50.7%) negative to positive IMF $B_y$ reversals.

### 3.3 Response time

Using the IMF $B_y$ reversals identified in section 3.2, we identified the coincident magnetic field data from the magnetotail spacecraft. The *Shue et al.* [1997] modeled magnetopause location was determined for each individual data point, and any data falling outside this modeled magnetopause location were discarded. Although this approach is prone to inaccuracies in the magnetopause model, it is convenient and statistically valid [e.g. *Case and Wild*, 2013]. Additionally, the data were further restricted to the region of the magnetotail most likely to contain the neutral sheet, i.e. $X_{GSW} < -5R_E$, $|Y_{GSW}| < 30R_E$, and $|Z_{GSW}| < 3R_E$. To increase the chances of detecting a neutral sheet crossing in the magnetospheric data, only intervals where at least one spacecraft recorded a reversal in the local $B_x$ component (i.e. passes through the neutral sheet) are kept. Intervals are four hours in length, centered around the IMF $B_y$ reversal. To ensure sufficient magnetospheric data surrounding a reversal, we require that the interval contains at least 120 data points (2 hours worth) of magnetospheric data. Intervals with fewer than 120 data points were discarded.

Using these criteria, 382 intervals of magnetotail data relating to 181 unique IMF $B_y$ reversals were identified. The data for each of these intervals were then manually inspected to determine if any neutral sheet response could be identified. We analysed the $B_x$ component of the local magnetic field for any sudden deviations occurring near the IMF $B_y$ reversal. We required that the polarity of the local $B_x$ either switch or the strength significantly reduce/increase and remain stable after the deviation (i.e. not switching back and forth between polarities). Additionally, we required that the deviations had to be clear and be complete within 10 min. We found the deviations were often accompanied by a matching deviation in the local $B_y$ component. These criteria ensure that sudden swaps in the polarity of the local $B_x$ component are the result of the neutral sweeping over the spacecraft. Additionally sudden increases or decreases in the magnitude of the local $B_x$ suggest that the neutral sheet has moved closer or further away from the spacecraft.

To reduce the chance of these changes occurring simply due to the spacecraft's orbit, rather than the motion of the neutral sheet, intervals where the spacecraft crossed the $Y = 0$ or $Z = 0$ axis were excluded, since one might expect a reversal in local $B_x$ in these cases anyway. Additionally, any gradual changes in $B_x$, which is indicative of a spacecraft's orbit passing through a somewhat stationary neutral sheet, were ignored.

An example of an IMF $B_y$ reversal with an associated abrupt change in the local $B_x$ component is shown in Figure 5. This example is of a positive to negative IMF $B_y$ reversal that took place at 07:54 UT on 28 February 1996. Plotted in the top row of Figure 5 is the trajectory of the Geotail spacecraft in the GSW X-Y, Y-Z, and X-Z planes respectively. Also plotted is an illustration of the expected clockwise neutral sheet rotation with this type of IMF $B_y$ reversal. As noted before, the spacecraft does not cross $Y = 0$ or $Z = 0$ axes and

remains in approximately the same region of space during the one hour preceding and three hours following the IMF $B_y$ reversal.

Plotted in the second row are (left) the IMF $B_x$ (red), $B_y$ (blue) and $B_z$ (green) components and (right) the AL index [*Davis and Sugiura*, 1966]. As indicated by the vertical red line, the IMF $B_y$ component reverses direction, swapping from around +2nT to around -2nT at 07:54 UT. We note the time given here is approximate, with the $B_y$ component first starting to drop in magnitude a few minutes earlier. The AL index remains at fairly quiet levels until around 50 mins after the reversal has occurred, thus suggesting substorm activity, for example, is not playing a large role in this interval.

In the following rows of Figure 5, the $x$, $y$, and $z$-components of the (left) local magnetic field and (right) perpendicular ion velocity are plotted. As indicated by the blue line, the magnetospheric spacecraft (Geotail) records a local $B_x$ component reversal at 08:20 UT, approximately 25 min after the IMF $B_y$ component reversal. The local $B_y$ component seems to match the orientation of the IMF $B_y$ component, being positive before the reversal and negative after the reversal on average. We note the local $B_z$ is steadily dropping as the spacecraft's orbit drops but remains at around +4nT when the local $B_x$ reversal occurs. Note, the sudden reversal of the local $B_z$ (from positive to negative) earlier in the interval, at around 07:35 UT, and data from Geotail's LEP instrument (not shown) is indicative of a magnetosheath flow - suggesting the spacecraft momentarily passed into the sheath.

The statistical results of these individual analyses are presented in Figure 6. Plotted in the top two panels are the locations of 120 observed sudden deviations in the local $B_x$ component for (left) positive to negative IMF $B_y$ reversals (54%) and (right) negative to positive reversals (46%). Plotted in red are events where the local $B_x$ component becomes more positive, i.e. $B_x$ switches from negative to positive, or remains negative but suddenly decreases in strength, or is positive and suddenly increases in strength. Plotted in blue are events where the local $B_x$ component becomes more negative. The direction of the expected neutral sheet twist, based on the IMF $B_y$ orientation, in each case is shown by the arrows.

For the positive to negative IMF $B_y$ reversals, we expect the majority of points in the $Y_{GSW} > 0$ sector to be red and the majority of points in the $Y_{GSW} < 0$ to be blue, since this would be indicative of a clockwise rotation. Conversely, for the negative to positive reversals we would expect the opposite since this would be indicative of an anti-clockwise rotation. Indeed, this appears to be the case, particularly beyond $|Y_{GSW}| > 5R_E$.

Plotted in the second row of panels (left) is a histogram of the response time, i.e. the time delay between the observed IMF $B_y$ reversal and the deviation in the local $B_x$ component. We find that the median response time is 17 min with a skewed distribution to shorter response times. Both types of $B_x$ deviations share a similar distribution.

Plotted in the subsequent panels are the location of the deviations in (left-right, top-bottom) $X$ ($R_E$), $|Y|$ ($R_E$), $|Z|$ ($R_E$), $|YZ|$ ($R_E$), and $r$ ($R_E$), where $|YZ| = \sqrt{Y^2 + Z^2}$ and $r = \sqrt{X^2 + Y^2 + Z^2}$ (all in GSW coordinate system). Also shown in each of the plots is the Spearman correlation coefficient and the linear lines of best fit (red for "more positive" data, blue for "more negative" data, and black for all data). We find that there is a weak correlation between the response times and the location of the deviation in the $X$-coordinate and radial distance ($r$) ($\sigma = -0.31$ and 0.32 respectively). We note that there is significant spread in the data, which is likely due to the local effects that play a significant role in the response time of the neutral sheet to reversals in the IMF $B_y$ component [*Sergeev et al.*, 2003].

## 4 Discussion

It is well known that Earth's magnetosphere responds to changes in the IMF orientation and, in particular, to changes in the IMF $B_y$ component. The idea of a neutral sheet responding to such changes, via a twist, was first introduced by *Russell* [1972] and *Cowley* [1981]

and confirmed by numerous studies thereafter. What has been lacking until now, however, is a large-scale statistical study of the neutral sheet response, particularly its timing, to reversals in the IMF $B_y$ orientation.

The statistical response of the neutral sheet to the IMF $B_y$ orientation is demonstrated in Figures 2 and 3. By averaging the local $B_x$ and $B_y$ components over 60 min, between $\pm 3\, R_E Z_{GSW}$, we find the average direction of $B_x$ and $B_y$ in the different spatial regions. A neutral sheet with no twist or rotation should average to $B_x = 0$ across this plane with equal flux of negative (tailward) and positive (earthward) $B_x$. The dominance of one direction of $B_x$ in one sector and the dominance of the opposite direction in the other, especially when that dominance is reversed depending upon the IMF $B_y$ orientation, illustrates a large scale twisting of the neutral sheet.

This is clearly illustrated, with a dominance of negative $B_x$ in the pre-midnight sector and a dominance of positive $B_x$ in the post-midnight sector for eastward IMF ($B_y > 0, |B_y| > |B_z|$). This is accompanied by a complete reversal of this trend for westward IMF ($B_y < 0, |B_y| > |B_z|$). Additionally, we find that the local $B_y$ component statistically matches the driving IMF conditions. This demonstrates that a positive IMF $B_y$ component twists the neutral sheet in an anti-clockwise motion (when visualised looking downtail from Earth). Conversely, a negative IMF $B_y$ component twists the neutral sheet in a clockwise motion. We note that the axis of the twist appears to be a little offset from 24 MLT (i.e. $Y_{GSW} = 0$), instead centered around 23 MLT, suggesting that there are some asymmetry effects also at work. Interestingly, this appears to align with the median location of substorm onset [e.g. *Nagai*, 1982; *Frey et al.*, 2004].

The twisting is most obvious during IMF $B_y$ dominated intervals (i.e. eastward and westward) but can also be seen during intervals with a non-zero IMF $B_z$ component (e.g. south-westward). Visual inspection seems to suggest that the twist is slightly more prominent under partly northward intervals versus partly southward intervals (e.g. north-west versus south-west). This matches with previous studies, e.g. *Owen et al.* [1995], who suggest that southward IMF results in high levels of geomagnetic activity which restrains the twisting of the neutral sheet. Indeed, we find that under purely southward IMF the neutral sheet is extremely disturbed with substantial variance in the local $B_x$ and $B_y$ components.

The interpretation of asymmetric flux loading in the tail lobes is supported by the direction of the plasma flows in the lobes. As shown in Figure 4, we observe duskward flows in the Northern Hemisphere and dawnward flows in the Southern Hemisphere under eastward IMF. This trend is reversed under westward IMF. These results are consistent with the work of *Haaland et al.* [2008].

When analyzing individual response times of the neutral sheet to IMF $B_y$ reversals, we found that the responses were on much shorter timescales than the large, statistical twist. Indeed, rather than responses of the order of 60-90 min (i.e. for a *Cowley* [1981] type twist), the responses were found to be centered around 17 min. This does not, however, rule out the longer timescale response, rather just suggesting that the shorter time scale is more obvious to see in individual analyses at the locations being sampled by the spacecraft.

The neutral sheet response times we present here include the propagation time of the solar wind/IMF from the bowshock to the magnetopause. The exact timing of this propagation through the magnetosheath varies, though is approximately 4-5 min [Khan and Cowley, 1999; *Wild et al.*, 2009], resulting in response times from the magnetopause of around 12-13 min. This result is consistent with the timescale proposed by *Tenfjord et al.* [2015], around 15 min from the bowshock or 10 min from the magnetopause, for pressure induced $B_y$ induction. Further, we note that *Wing et al.* [2002] found that the nightside magnetic field, at geosynchronous orbit, responded to southward turnings in the IMF within 12 min. Modeling by *Tenfjord et al.* [2015] suggest that the rapid induction of the IMF By component onto closed field lines is driven by fast-mode waves, which can travel at 900km/s, carrying

the magnetic pressure information into the lobes. Further investigation into this seems warranted.

Additionally, we note that, as shown in the histogram of Figure 6, some of the "responses" seem to occur before the IMF $B_y$ component actually reversed. Rather than indicating that the IMF was not the driver of the change, we suggest that there were perhaps inaccurate solar wind propagation delays or that there were localized features and bulges related to internal processes in the plasmasheet (e.g. substorms, and reconnection events) causing local topological changes.

There appears to be little dependence on the neutral sheet response time based on the location on the sheet. Only a weak correlation was found with radial distance along the neutral sheet ($\sigma = 0.32$). We suggest that this weak correlation is most likely due to the local variability inherent with the location and dynamics of the neutral sheet. Indeed, when we attempted to perform a superposed epoch analysis of the response times, we found significant variance that rendered the result inconclusive.

## 5 Conclusions

In this study, we collated magnetotail magnetic field data, spanning 25 years and from a range of magnetospheric spacecraft missions, with the aim of determining the response of the neutral sheet to changes in the IMF $B_y$ component. The magnetic field data were converted into the GSW coordinate system to account for aberration effects, filtered to our region of interest, and normalized using dynamic pressure.

As shown in Figure 2, the neutral sheet develops a twist under non-zero IMF $B_y$ conditions. Under sustained positive IMF $B_y$ conditions, the neutral sheet twists (rotates) in an anti-clockwise motion (when visualised looking downtail from Earth). Conversely, sustained negative IMF $B_y$ twists the neutral sheet in a clockwise motion. We find that this is slightly more apparent under northward IMF conditions than southward. As shown in Figure 3, we also find that the local $B_y$ component strongly matches the driving IMF $B_y$ orientation.

The proposed method for introducing a neutral sheet twist is unequal loading of magnetic flux into the tail lobes [e.g. *Cowley*, 1981]. This is supported by the plasma convection flows presented in Figure 4. We observe duskward flows in the northern hemisphere and dawnward flows in the southern hemisphere under positive IMF $B_y$ conditions. This pattern is reversed under negative IMF $B_y$ conditions.

When we analyzed the response time of the neutral sheet to reversals in the IMF $B_y$ component, however, we found the sheet responded on much shorter timescales than possible with the traditional Cowley twist. We believe this work provides evidence for an induced $B_y$ component on much shorter timescales, of the order of 10-20 min, as proposed by *Tenfjord et al.* [2015, 2016]. The time taken for this response did not strongly correlate to distance downtail.

From both the large-scale statistical response, and the shorter individual analyses, it seems apparent that the neutral sheet responds to the IMF $B_y$ component on multiple timescales.

**Acknowledgments**
We gratefully acknowledge the various instrument teams from each of the spacecraft missions used in this study. The Cluster and Double Star data were provided by ESA's Cluster Science Archive. The Geotail data are provided from the Data ARchives and Transmission System (DARTS) of the Institute of Space and Astronautical Science. The THEMIS data were provided by NASA Goddard Space Flight Center's CDAWeb. Solar wind data were provided by NASA GSFC's OMNIWeb database.

NAC and AG were supported during this study by STFC grant number ST/M001059/1. The work of TN at ISAS/JAXA was supported by MEXT/JSPS KAKENHI grant 17H06140.

## References

Angelopoulos, V., Kennel, C. F., Coroniti, F. V., Pellat, R., Kivelson, M. G., Walker, R. J., et al. (1994), Statistical characteristics of bursty bulk flow events, *J. Geophys. Res.*, *99*(A11), 21257–21280, doi:10.1029/94JA01263.

Auster, H.U., Glassmeier, K.H., Magnes, W., Aydogar, O., Baumjohann, W., Constantinescu, D., Fischer, D., Fornacon, K.H., Georgescu, E., Harvey, P. and Hillenmaier, O. (2009), The THEMIS fluxgate magnetometer, in *The THEMIS Mission*, 235–264, Springer New York.

Balogh, A., M. W. Dunlop, S. W. H. Cowley, D. J. Southwood, J. G. Thomlinson, K. H. Glassmeier, G. Musmann, H. Lühr, S. Buchert, M. H. Acuña, D. H. Fairfield, J. A. Slavin, W. Riedler, K. Schwingenschuh, and M. G. Kivelson (1997), The Cluster Magnetic Field Investigation, in The Cluster and Phoenix Missions, edited by C. P. Escoubet, C. T. Russell, R. Schmidt, 65–91, Springer Netherlands, Dordrecht, doi:10.1007/978-94-011-5666-0_3.

Browett, S. D., R. C. Fear, A. Grocott, and S. E. Milan (2016), Timescales for the penetration of IMF By into the Earth's magnetotail, *J. Geophys. Res. Space Physics*, *121*, doi:10.1002/2016JA023198.

Carr, C., et al. (2005), The Double Star magnetic field investigation: instrument design, performance and highlights of the first year's observations, *Annales Geophysicae*, *23*(8), 2713–2732, doi:10.5194/angeo-23-2713-2005

Case, N. A., and J. A. Wild (2012), A statistical comparison of solar wind propagation delays derived from multispacecraft techniques, *J. Geophys. Res.*, *117*, A02101, doi:10.1029/2011JA016946.

Case, N. A., and J. A. Wild (2013), The location of the Earth's magnetopause: A comparison of modeled position and in situ Cluster data, *J. Geophys. Res. Space Physics*, *118*, 6127–6135, doi:10.1002/jgra.50572.

Cowley, S.W.H., and W.J. Hughes (1983), Observation of an IMF sector effect in the Y magnetic field component at geostationary orbit, *Planetary and Space Science*, *31*(1),doi: 10.1016/0032-0633(83)90032-6.

Cowley, S. W. H. (1981), Magnetospheric asymmetries associated with the y-component of the IMF, *Planetary and Space Science*, *29*(1), 79–96, doi:10.1016/0032-0633(81)90141-0

Davis, T. N., and M. Sugiura (1966), Auroral electrojet activity index AE and its universal time variations, *J. Geophys. Res.*, *71*(3), 785–801, doi:10.1029/JZ071i003p00785.

Fairfield, D.H. (1980), A statistical determination of the shape and position of the geomagnetic neutral sheet, *Journal of Geophysical Research: Space Physics*, *85(A2)*, 775–780, doi:10.1029/JA085iA02p00775.

Frey, H. U., S. B. Mende, V. Angelopoulos, and E. F. Donovan (2004), Substorm onset observations by IMAGE-FUV, *J. Geophys. Res.*, *109*, A10304, doi: 10.1029/2004JA010607.

Grocott, A., T. K. Yeoman, S. E. Milan, O. Amm, H. U. Frey, L. Juusola, et al. (2007), Multi-scale observations of magnetotail flux transport during IMF-northward non-substorm intervals, *Annales Geophysicae*, *25*(7), 1709–1720, doi:10.5194/angeo-25-1709-2007

Haaland, S., G. Paschmann, M. Förster, J. Quinn, R. Torbert, H. Vaith, P. Puhl-Quinn, and C. Kletzing (2008), Plasma convection in the magnetotail lobes: statistical results from Cluster EDI measurements, *Ann. Geophys.*, *26*, 2371–2382, doi:10.5194/angeo-26-2371-2008.

Hammond, C. M., M. G. Kivelson, and R. J. Walker (1994), Imaging the effect of dipole tilt on magnetotail boundaries, *J. Geophys. Res.*, *99*(A4), 6079–6092, doi:10.1029/93JA01924.

Hones, E. W. , R. D. Zwickl, T. A. Fritz, S. J. Bame (1986), Structural and dynamical aspects of the distant magnetotail determined from ISEE-3 plasma measurements, *Planetary and Space Science*, *34*(10), 889–901, doi:10.1016/0032-0633(86)90001-2.

Khan, H. and S. W. H. Cowley (1999), Observations of the response time of high-latitude ionospheric convection to variations in the interplanetary magnetic field using EISCAT and IMP-8 data, *Ann. Geophys.*, *17*, 1306–1335

Khurana, K. K., R. J. Walker, and T. Ogino (1996), Magnetospheric convection in the presence of interplanetary magnetic ïňĄeld By: A conceptual model and simulations, *J. Geophys. Res.*, *101*, 4907–4916.

Kitaev, A.V. (1991), Diffusive penetration of the IMF By into the magnetosphere, *Planetary and Space Science*, *41*(2), doi:10.1016/0032-0633(93)90044-3

King, J. H., and N. E. Papitashvili (2005), Solar wind spatial scales in and comparisons of hourly Wind and ACE plasma and magnetic field data, *J. Geophys. Res.*, *110*, A02104, doi: 10.1029/2004JA010649.

Kokubun, S., T. Yamamoto, M. H. Acuña, K. Hayashi, K. Shiokawa, and H. Kawano (1994), The Geotail magnetic field experiment, *J. Geomag. Geoelec.*, *46*(1), 7–22.

McComas, D. J., C. T. Russell, R. C. Elphic, and S. J. Bame (1986), The near-Earth cross-tail current sheet: Detailed ISEE 1 and 2 case studies, *J. Geophys. Res.*, *91*(A4), 4287–4301, doi:10.1029/JA091iA04p04287.

Milan, S. E., A. Grocott, and B. Hubert (2010), A superposed epoch analysis of auroral evolution during substorms: Local time of onset region, *J. Geophys. Res.*, *115*, A00I04, doi:10.1029/2010JA015663.

Motoba, T., K. Hosokawa, Y. Ogawa, N. Sato, A. Kadokura, S. C. Buchert, and H. Rème (2011), In situ evidence for interplanetary magnetic field induced tail twisting associated with relative displacement of conjugate auroral features, *J. Geophys. Res.*, *116*, A04209, doi:10.1029/2010JA016206.

Nagai, T. (1982), Observed magnetic substorm signatures at synchronous altitude, *J. Geophys. Res.*, *87*(A6), 4405–4417, doi: 10.1029/JA087iA06p04405.

Nagai, T. (1987), Interplanetary magnetic field By effects on the magnetic field at synchronous orbit, *J. Geophys. Res.*, *92*(A10), 11215–11220, doi:10.1029/JA092iA10p11215.

Ness, N. F. (1965), The Earth's magnetic tail, *J. Geophys. Res.*, *70*(13), 2989–3005, doi:10.1029/JZ070i013p02989.

Nishida, A., T. Mukai, T. Yamamoto, S. Kokubun, and K. Maezawa (1998), A unified model of the magnetotail convection in geomagnetically quiet and active times, *J. Geophys. Res.*, *103*(A3), 4409–4418, doi:10.1029/97JA01617.

Owen, C. J., J. A. Slavin, I. G. Richardson, N. Murphy, and R. J. Hynds (1995), Average motion, structure and orientation of the distant magnetotail determined from remote sensing of the edge of the plasma sheet boundary layer with E > 35 keV ions, *J. Geophys. Res.*, *100*(A1), 185–204, doi:10.1029/94JA02417.

Park, K. S., T. Ogino, and R. J. Walker (2006), On the importance of antiparallel reconnection when the dipole tilt and IMF By are nonzero, *J. Geophys. Res.*, *111*, A05202, doi:10.1029/2004JA010972.

Paschmann, G., Melzner, F., Frenzel, R. et al. (1997), The electron drift instrument for Cluster, *Space Science Reviews*, *79*(233), doi:10.1023/A:1004917512774

Pitkänen, T., M. Hamrin, A. Kullen, R. Maggiolo, T. Karlsson, H. Nilsson, and P. Norqvist (2016), Response of magnetotail twisting to variations in IMF By: A THEMIS case study 1–2 January 2009, *Geophys. Res. Lett.*, *43*, 7822–7830, doi:10.1002/2016GL070068.

Rong, Z. J., A. T. Y. Lui, W. X. Wan, Y. Y. Yang, C. Shen, A. A. Petrukovich, Y. C. Zhang, T. L. Zhang, and Y. Wei (2015), Time delay of interplanetary magnetic field penetration into Earth's magnetotail. *J. Geophys. Res. Space Physics*, *120*, 3406–3414. doi: 10.1002/2014JA020452.

Russell, C. T. (1972), The configuration of the magnetosphere, in *Critical Problems of Magnetospheric Physics*, edited by E. R. Dyer, pp. 1–16, IUCSTP Secretariat, National Academy of Sciences, Washington, D. C.

Sergeev, V., and et al. (2003), Current sheet flapping motion and structure observed by Cluster, *Geophys. Res. Lett.*, *30*(6), 1327, doi:10.1029/2002GL016500.

509 Shue, J.-H., J. K. Chao, H. C. Fu, C. T. Russell, P. Song, K. K. Khurana, and H. J. Singer
510 (1997), A new functional form to study the solar wind control of the magnetopause size
511 and shape, *J. Geophys. Res.*, *102*(A5), 9497–9511, doi:10.1029/97JA00196.
512 Sibeck, D. G., G. L. Siscoe, J. A. Slavin, E. J. Smith, B. T. Tsurutani, and R. P. Lepping
513 (1985), The distant magnetotail's response to a strong interplanetary magnetic field
514 $B_y$: Twisting, flattening, and field line bending, *J. Geophys. Res.*, *90*(A5), 4011–4019,
515 doi:10.1029/JA090iA05p04011.
516 Speiser, T. W., and N. F. Ness (1967), The neutral sheet in the geomagnetic tail: Its motion,
517 equivalent currents, and field line connection through it, *J. Geophys. Res.*, *72*(1), 131–141,
518 doi:10.1029/JZ072i001p00131.
519 Tenfjord, P., N. Østgaard, K. Snekvik, K. M. Laundal, J. P. Reistad, S. Haaland, and S. E.
520 Milan (2015), How the IMF By induces a By component in the closed magnetosphere and
521 how it leads to asymmetric currents and convection patterns in the two hemispheres, *J.*
522 *Geophys. Res. Space Physics*, *120*, 9368–9384, doi:10.1002/2015JA021579.
523 Tenfjord, P., N. Østgaard, R. Strangeway, S. Haaland, K. Snekvik, K. M. Laundal, J. P. Reis-
524 tad, and S. E. Milan (2016), Magnetospheric response and reconfiguration times following
525 IMF By reversals, *J. Geophys. Res. Space Physics*, *122*, doi:10.1002/2016JA023018.
526 Tsyganenko, N. A., S. B. P. Karlsson, S. Kokubun, T. Yamamoto, A. J. Lazarus, K. W.
527 Ogilvie, C. T. Russell, and J. A. Slavin (1998), Global configuration of the magnetotail
528 current sheet as derived from Geotail, Wind, IMP 8 and ISEE 1/2 data, *J. Geophys. Res.*,
529 *103*(A4), 6827–6841, doi:10.1029/97JA03621.
530 Tsyganenko, N. A., and D. H. Fairfield (2004), Global shape of the magnetotail cur-
531 rent sheet as derived from Geotail and Polar data, *J. Geophys. Res.*, *109*, A03218,
532 doi:10.1029/2003JA010062.
533 Wang, J. Y., C. Wang, Z. H. Huang, and T. R. Sun (2014), Effects of the interplanetary mag-
534 netic field on the twisting of the magnetotail: Global MHD results, *J. Geophys. Res. Space*
535 *Physics*, *119*, 1887–1897, doi:10.1002/2013JA019257.
536 Wilcox, J. M. (1972), Inferring the interplanetary magnetic field by observing the polar geo-
537 magnetic field, *Rev. Geophys.*, *10*(4), 1003–1014, doi: 10.1029/RG010i004p01003.
538 Wild, J. A., E. E. Woodfield and S. K. Morley (2009), On the triggering of auroral substorms
539 by northward turnings of the interplanetary magnetic field, *Ann. Geophys.*, *27*(9), 3559–
540 3570, doi:10.5194/angeo-27-3559-2009
541 Wing, S., P. T. Newell, D. G. Sibeck, and K. B. Baker (1995), A large statistical study of the
542 entry of interplanetary magnetic field YâĂŘcomponent into the magnetosphere, *Geophys.*
543 *Res. Lett.*, *22*(16), 2083–2086, doi:10.1029/95GL02261.
544 Wing, S., D. G. Sibeck, M. Wiltberger, and H. Singer, Geosynchronous magnetic field
545 temporal response to solar wind and IMF variations, *J. Geophys. Res.*, *107*(A8), doi:
546 10.1029/2001JA009156, 2002.
547 Xiao, S., T. Zhang, Y. Ge, G. Wang, W. Baumjohann, and R. Nakamura (2016), A statistical
548 study on the shape and position of the magnetotail neutral sheet, *Ann. Geophys.*, *34*, 303–
549 311, doi:10.5194/angeo-34-303-2016.
550 Zhang, T. L., W. Baumjohann, R. Nakamura, A. Balogh, and K.-H. Glassmeier (2002), A
551 wavy twisted neutral sheet observed by CLUSTER, *Geophys. Res. Lett.*, *29*(19), 1899,
552 doi:10.1029/2002GL015544.

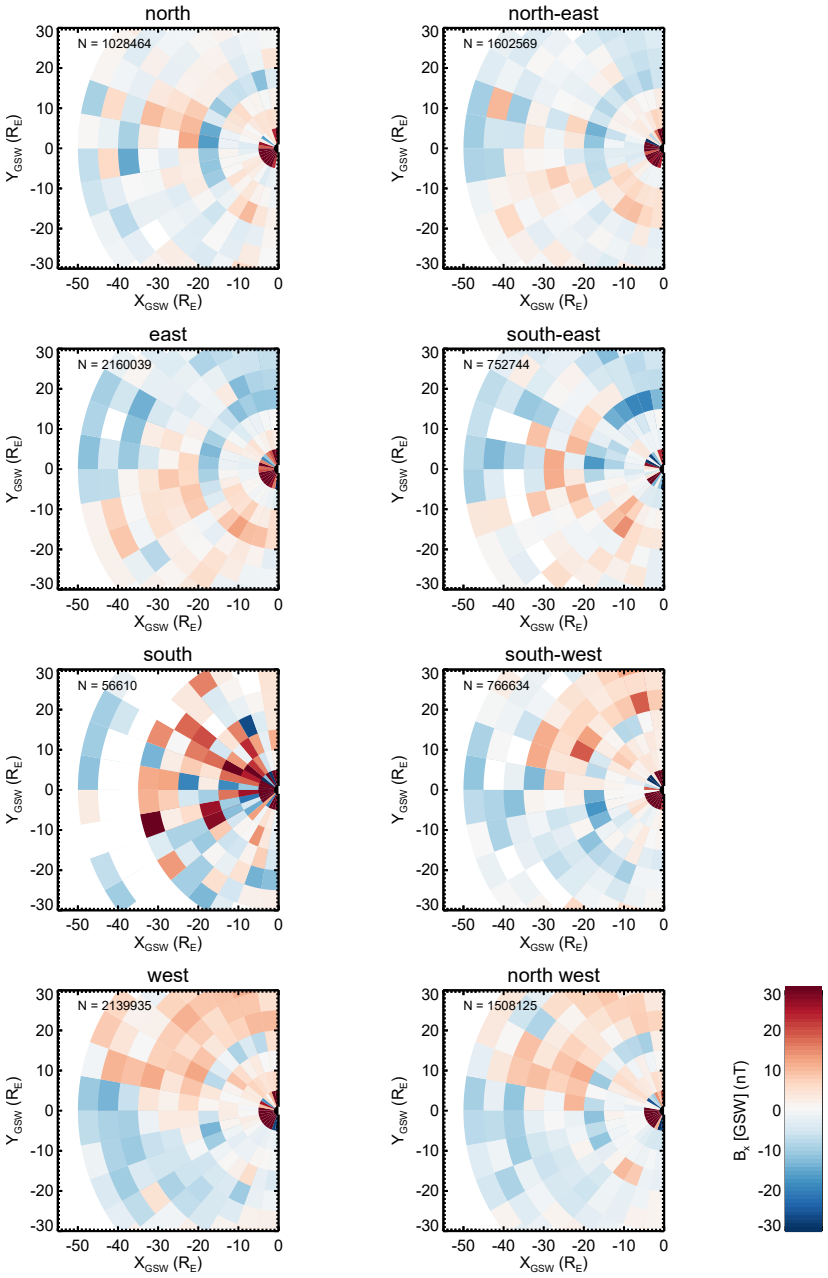


147 **Figure 2.** The local magnetic field $B_x$ component data, recorded between $\pm 3\,R_E$ in the Z-direction (GSW
148 coordinates), are sorted into panels by the 60 min average solar wind clock angle direction. Individual bins in
149 each panel are colored by the median $B_x$ in that bin. The number of data within each panel is also shown.

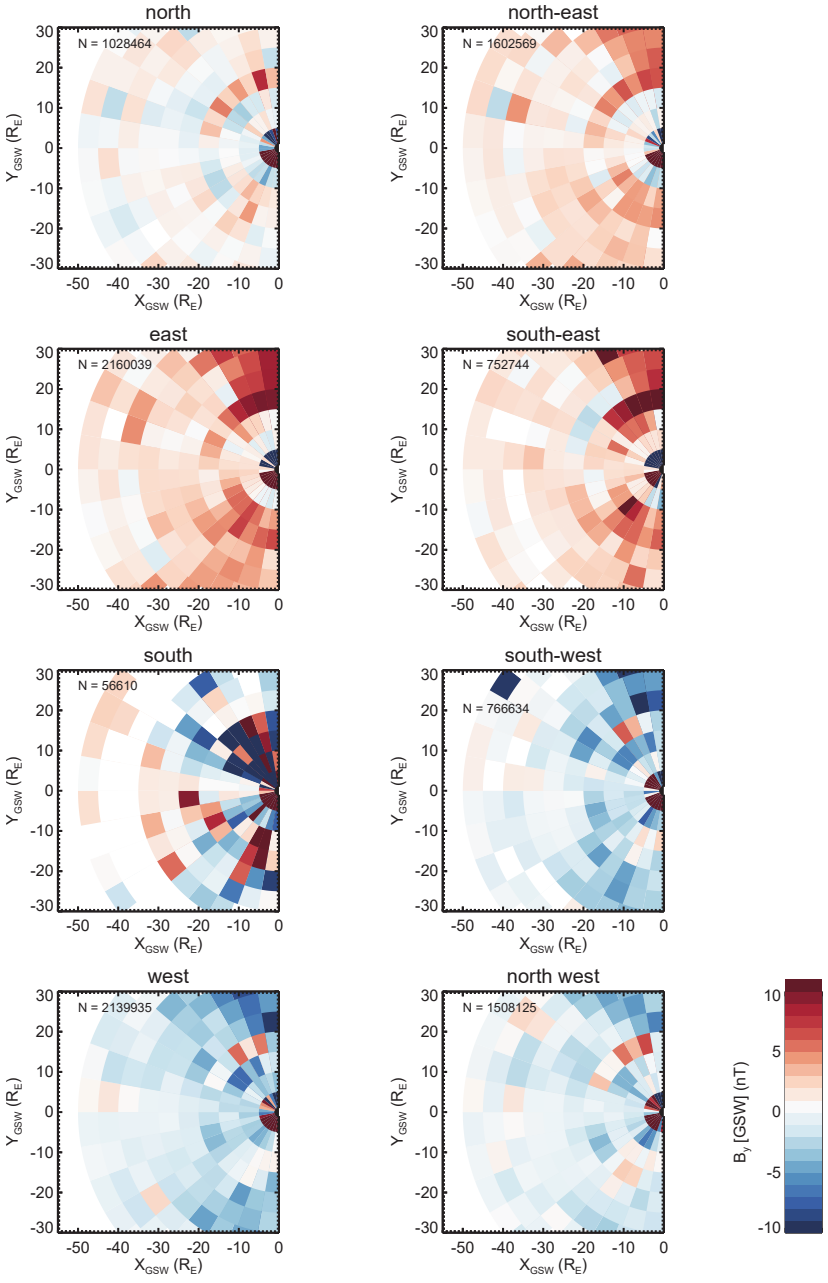


**Figure 3.** The local magnetic field $B_y$ component data are plotted in the same format as Figure 2. Note the scale has changed from ±30 nT to ±10 nT.

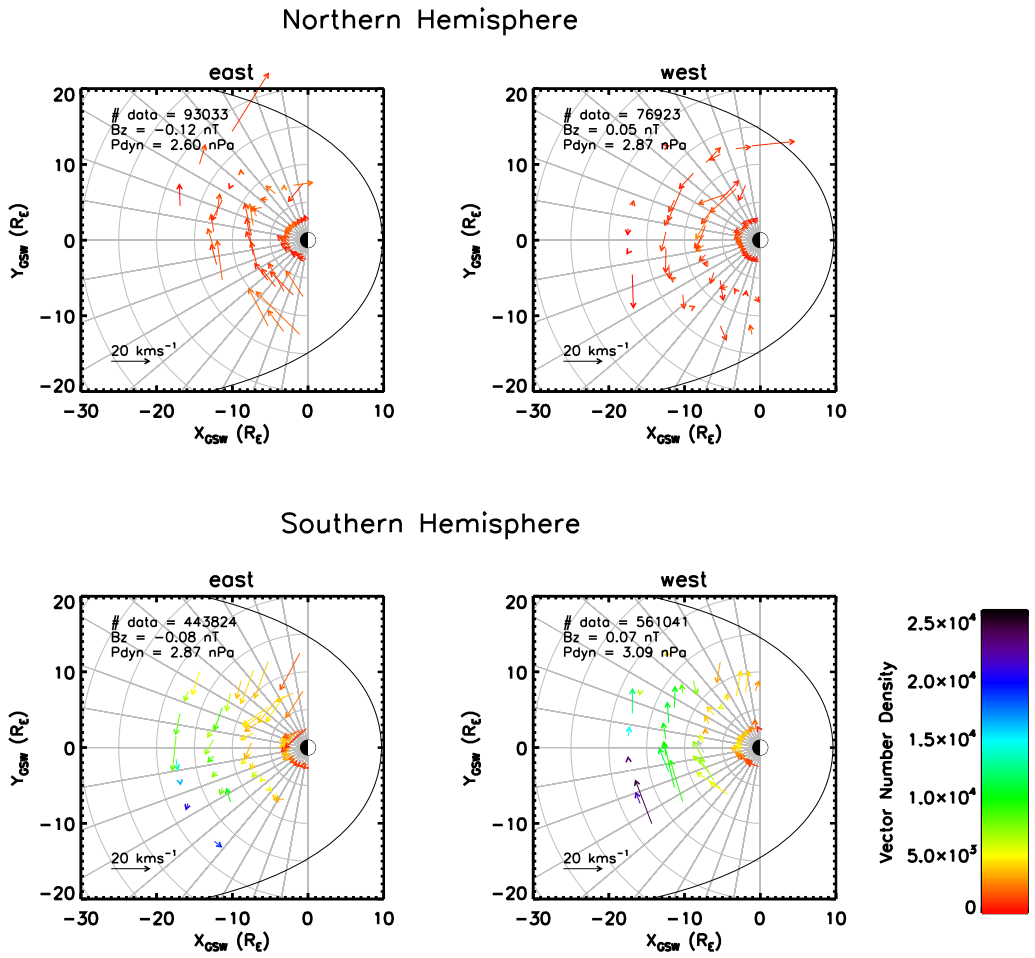


**Figure 4.** Cluster EDI velocity data, recorded from within the nightside magnetotail lobes, are sorted by IMF clock angle orientation. For both the northern and southern hemispheres, the mean $V_{xy}$ in each bin is presented under eastward and westward IMF orientation. The mean $V_{xy}$ magnitude in each bin is indicated by the length of the arrow. The color of each arrow indicates the number of vectors in that bin.

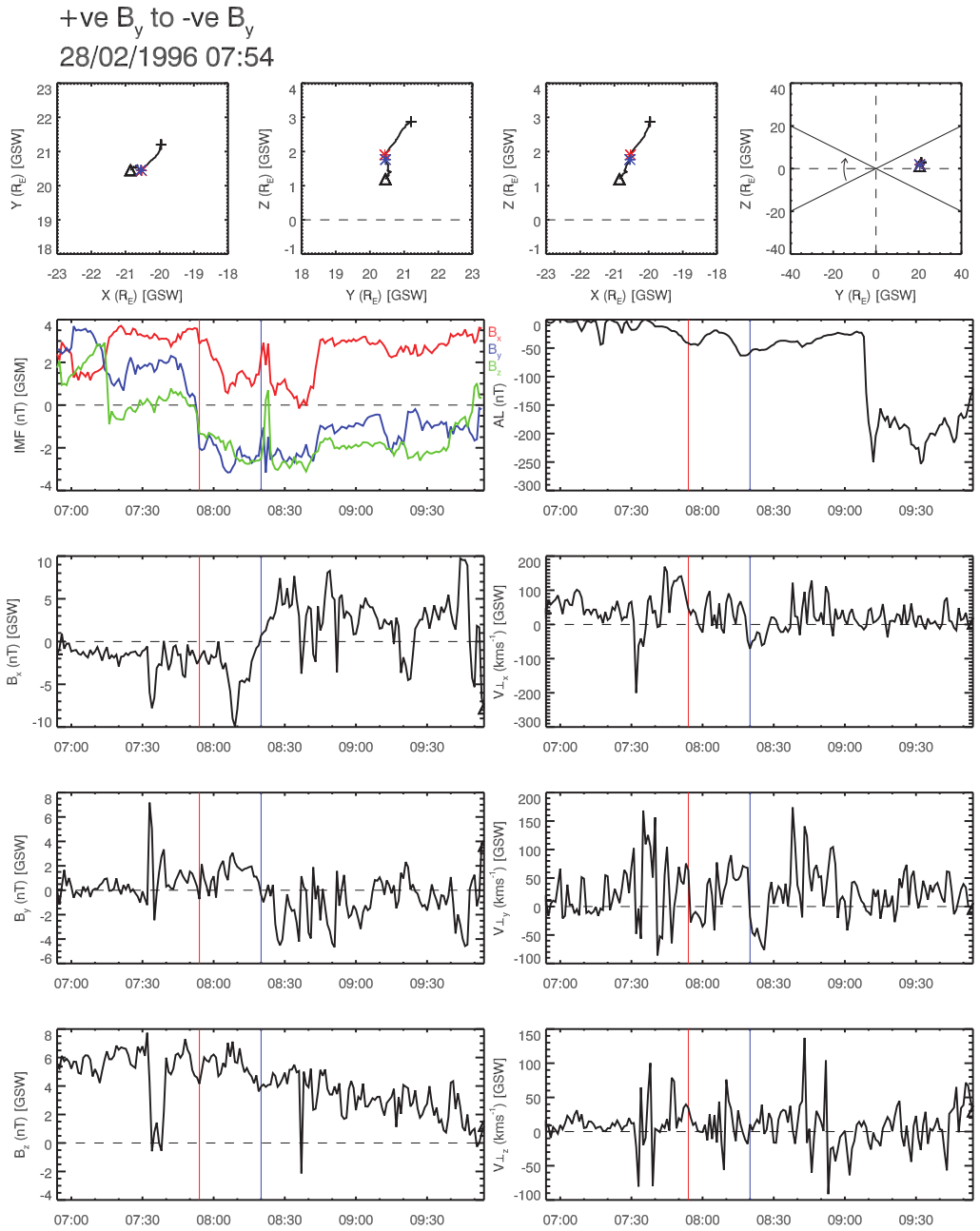


**Figure 5.** An example interval of near neutral sheet data associated with a positive to negative IMF $B_y$ reversal. Plotted in the top row is the spacecraft trajectory in the GSW X-Y, Y-Z, and X-Z planes. Also plotted is an illustration of the expected neutral sheet rotation with this type of IMF $B_y$ reversal. Plotted in the second row are (left) the IMF $B_x$ (red), $B_y$ (blue) and $B_z$ (green) components and (right) the AL index. In the following rows, the x,y, and z components of the (left) local magnetic field and (right) perpendicular ion velocity are plotted. The red asterisks and lines indicate when the IMF $B_y$ reversal took place; the blue asterisks and lines indicate when the local $B_x$ reversal occurred.

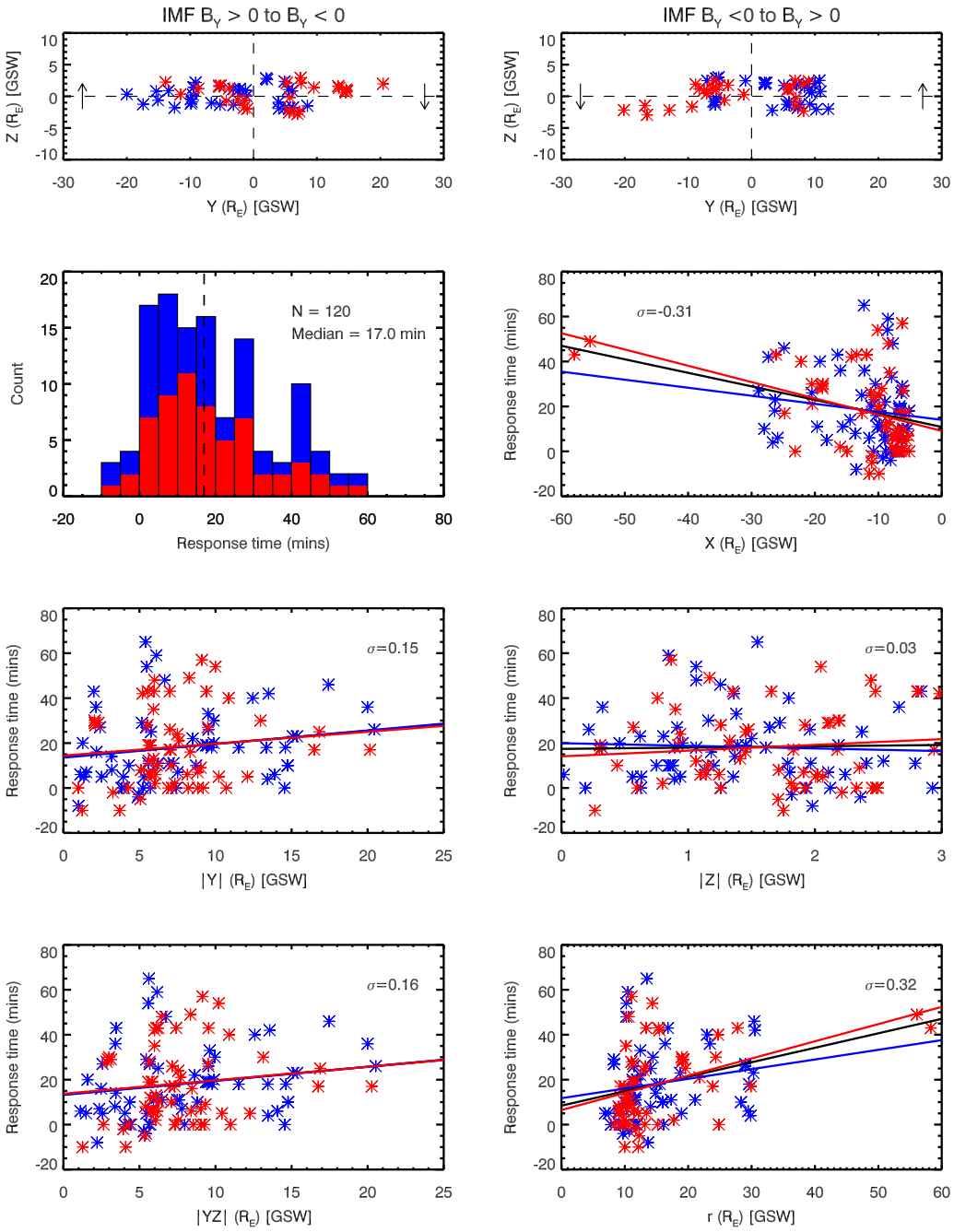


**Figure 6.** Plotted are the locations and response times of the neutral twisting after a reversal in the IMF $B_y$ component. Plotted in red are events where the local $B_x$ component becomes more positive, i.e. $B_x$ switches from negative to positive, or remains negative but suddenly decreases in strength, or is positive and suddenly increases in strength. Plotted in blue are events where the local $B_x$ component becomes more negative. Shown in the response time vs location plots is the correlation coefficient for the data.